



**HAL**  
open science

# A tight-binding atomistic approach for point defects and surfaces applied to the o-Al<sub>13</sub>Co<sub>4</sub> quasicrystalline approximant

Oussama Bindech, Christine Goyhenex, Émilie Gaudry

## ► To cite this version:

Oussama Bindech, Christine Goyhenex, Émilie Gaudry. A tight-binding atomistic approach for point defects and surfaces applied to the o-Al<sub>13</sub>Co<sub>4</sub> quasicrystalline approximant. *Computational Materials Science*, 2021, 200, pp.110826. 10.1016/j.commatsci.2021.110826 . hal-03454409v2

**HAL Id: hal-03454409**

**<https://hal.science/hal-03454409v2>**

Submitted on 29 Nov 2021

**HAL** is a multi-disciplinary open access archive for the deposit and dissemination of scientific research documents, whether they are published or not. The documents may come from teaching and research institutions in France or abroad, or from public or private research centers.

L'archive ouverte pluridisciplinaire **HAL**, est destinée au dépôt et à la diffusion de documents scientifiques de niveau recherche, publiés ou non, émanant des établissements d'enseignement et de recherche français ou étrangers, des laboratoires publics ou privés.

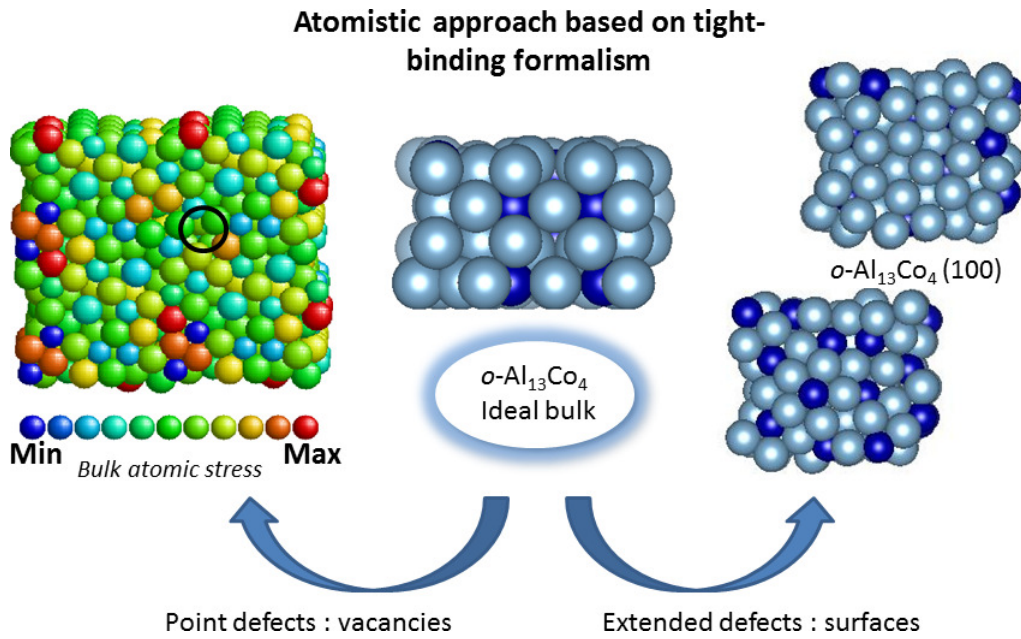


Distributed under a Creative Commons Attribution - NonCommercial - NoDerivatives 4.0 International License

# Graphical Abstract

A tight-binding atomistic approach for point defects and surfaces applied to the  $\sigma\text{-Al}_{13}\text{Co}_4$  quasicrystalline approximant

O. Bindech, C. Goyhenex, É. Gaudry



## Highlights

### **A tight-binding atomistic approach for point defects and surfaces applied to the o-Al<sub>13</sub>Co<sub>4</sub> quasicrystalline approximant**

O. Bindech, C. Goyhenex, É. Gaudry

- A tight-binding N-body potential for Al-Co interactions is implemented.
- We model the o-Al<sub>13</sub>Co<sub>4</sub> quasicrystalline approximant in the presence of atomic vacancies and surfaces.
- The importance of stress relaxation in vacancies formation in bulk o-Al<sub>13</sub>Co<sub>4</sub> is highlighted thanks to an atomic stress mapping.
- A good agreement between DFT and semi-empirical calculations is obtained for surface structures and relative surface energies.

# A tight-binding atomistic approach for point defects and surfaces applied to the $\alpha$ -Al<sub>13</sub>Co<sub>4</sub> quasicrystalline approximant

O. Bindech<sup>a</sup>, C. Goyhenex<sup>a,\*</sup>, É. Gaudry<sup>b</sup>

<sup>a</sup>*Institut de Physique et Chimie des Matériaux de Strasbourg, Université de Strasbourg, CNRS UMR 7504, 23 rue du Loess, BP 43, Strasbourg, F-67034, France*

<sup>b</sup>*Univ. Lorraine, CNRS, Institut Jean Lamour, 2 allée André Guinier, Nancy, F-54000, France*

---

## Abstract

We implemented an N-body potential for the Al-Co interactions and applied it to the  $\alpha$ -Al<sub>13</sub>Co<sub>4</sub> quasicrystalline approximant. We show its ability to model this complex compound in the presence of point and extended defects (atomic vacancies and surfaces). The importance of stress relaxation in vacancy formation is highlighted through the mapping of local pressures in the bulk compound. Thanks to the many body character of the potential, the surfaces could be investigated which was not done before in atomistic studies of this complex phase. Our classical simulations point up the competition between preserving the cohesion by minimizing the number of broken bonds and avoiding the presence of Co atoms at the surface. This study opens the way to large scale simulations of phenomena involving complex metallic alloys in particular at their surfaces.

*Keywords:* N-body potential, DFT, aluminum, cobalt, quasicrystalline approximant, point defects, surface

---

\*Corresponding author

*Email address:* `christine.goyhenex@ipcms.unistra.fr` (C. Goyhenex)

## 1. Introduction

The  $\text{Al}_{13}\text{Co}_4$  intermetallic compound has recently attracted the attention of many research groups due to its unusual physical and chemical properties. A few examples include its strongly anisotropic magnetic and electronic transport behavior [1], its interesting catalytic performances towards hydrogenation reactions [2, 3], as well as its unexpected wetting properties [4]. To understand these fascinating features, the determination of structure-properties relationships is crucial. This task is however challenging, since defects play a non negligible role in this compound. For instance, the lack of quantitative agreement between the *ab initio*-calculated theoretical transport coefficients and the experiments have been attributed, at least in part, to the presence of disorder in the samples [1]. More recently, emphasis was raised on the fact that experimental phonon lifetimes and temperature-independent lattice thermal conductivity in  $\text{Al}_{13}\text{Co}_4$  can only be fully described by properly taking into account the disorder [5].

The orthorhombic  $\text{o-Al}_{13}\text{Co}_4$  crystal structure was primarily refined in the  $Pmn2_1$  space group using X-ray diffraction (XRD) experiments [6]. Early identified as a quasicrystal approximant [7],  $\text{o-Al}_{13}\text{Co}_4$  presents all structural features characteristic of a Complex Metallic Alloy (CMA) [8], including a crystal cell containing more than 100 atoms, arranged in well-defined bipentagonal polyhedra, and the occurrence of inherent disorder, probed by the large atomic displacement parameters of several aluminum positions. Recently, high-resolution single-crystal XRD with spherical aberration corrected HRTEM and HRSTEM (High Resolution Transmission and Scanning Transmission Electron Microscopy) has revealed multiple split and partially occupied crystallographic sites. [9]

Accurate and reliable modelling of  $\text{o-Al}_{13}\text{Co}_4$  where structural complexity and local disorder are at play, requires large computational cells. Thus, in this case, computational limitations prevent Density Functional Theory calculations from being applied to perform atomistic simulations. Alternative methods based on interatomic potentials are more suitable for this purpose. Such approaches have already been successfully used to model bulk  $\text{o-Al}_{13}\text{Co}_4$  characteristics, like thermodynamic [10, 11] and vibrational [5, 12] properties, based on oscillating pair potentials derived from force or/and energy matching to *ab initio* calculations [13]. However, the transferability of the previous

potentials built for bulk systems, to other properties related to the presence of surfaces, is not trivial. Indeed, pair potentials are insensitive to changes in coordination and thus, are not *a priori* suited to catch the increased bond strength of atoms at or near surfaces due to their strongly reduced average coordination. Because of the strong practical interests on  $\text{Al}_{13}\text{Co}_4$  surfaces, like chemical reactivity [14], wetting [4], oxidation resistance [15], the question of the transferability of Al-Co pair potentials to surface properties is of interest. As far as we know, the few parameterized potentials built for bulk Al-Co alloys [16, 17, 18, 19] are not evaluated against surface properties. On the other hand, studies involving metallic surfaces mainly relate to experimental observations combined with DFT. The latter is used to quantify the relative stability between different configurations[20, 21, 22, 14].

We therefore propose here to move a step forward towards the modeling at the atomic scale of complex intermetallics including their surfaces by developing a new parameter set for Al-Co alloys using a simple many body interatomic potential. This potential based on the tight-binding formalism is founded on the fitting to *ab initio* data calculated for pure Co, pure Al and several Al-Co alloy phases including o- $\text{Al}_{13}\text{Co}_4$ . The new parameter set is applied to the study of the formation of Al bulk vacancies and the o- $\text{Al}_{13}\text{Co}_4(100)$  surface which are two archetypes of respectively point and extended defects.

## 2. Materials and Methods

### 2.1. Computational details

#### 2.1.1. Tight-Binding potentials

The bonding in (Al, Co) based systems was modeled by using a tight-binding (TB)  $N$ -body potential based on the second moment approximation of the density of states in the Tight-Binding formalism (TB-SMA)[23, 24]. It is derived from a simplified but realistic description of the electronic structure and has been widely used for a large set of metals and alloys, mostly of the transition series[24, 25]. It was also extended with success to metals having a free-electron-like character. [26, 27] In the case of Al, the relevance of TB was attributed to the fact that d orbitals play a non negligible role in the electronic structure of the material.[28] This semi-empirical potential is also well known to accurately describe the relaxations and reconstructions at surfaces or adlayers. [29, 30, 31, 32] Within the TB-SMA, the total energy

at a site  $i$  of a system of atoms writes as the sum of an attractive band term  $E_i^b$ , derived from the electronic structure, and a repulsive Born-Mayer one ( $E_i^r$ ):

$$E_i = E_i^b + E_i^r = -\sqrt{\xi^2 \sum_j e^{-2q(\frac{r_{ij}}{r_0}-1)}} + \sum_j A e^{-p(\frac{r_{ij}}{r_0}-1)} \quad (1)$$

Then the total energy is the sum of energies  $E_i$  over sites  $i$ . For homoatomic interactions,  $r_0$  is the next nearest neighbor distance at equilibrium in the considered pure material. For mixed interactions it is taken as the arithmetic average between the values of the two pure corresponding materials. The parameters  $A, \xi, p, q$  are fitted in order to reproduce the physical properties of reference materials. In addition, we have to fix a cut-off radius  $r_c$  for the interactions. Typically, in a bimetallic material,  $r_c$  is taken as the second neighbor distance for the bulk material of the largest atom. Then, the potential is linked up to zero at higher order neighbors with a fifth-order polynomial in order to avoid discontinuities in calculated quantities like energies and forces.

Such an analytical formulation can easily be implemented in classical Molecular Dynamics (MD) or Monte Carlo simulations. In the present work, a quenched molecular dynamics (QMD) method has been used as a relaxation procedure to optimize the crystal structure at  $T = 0$  K. It means that the equations of motion are solved for atoms  $i$  while cancelling their velocity  $v_i$ , when the product  $\vec{F}_i \cdot \vec{v}_i$  is negative.

### 2.1.2. Density Functional Theory

Electronic structure calculations were performed within the density functional theory (DFT) implemented in the plane wave Vienna *ab initio* simulation package (VASP) [33, 34, 35, 36]. The projector-augmented wave (PAW) method [37, 38] and the spin-polarized generalized gradient approximation (GGA-PBE) [39, 40] were used in this work. Nine valence electrons were explicitly treated for Co ( $4s^1 3d^8$ ) and three for Al ( $3s^2 3p^1$ ). Total energies were minimized until the energy differences became less than  $10^{-6}$  eV between two electronic cycles during the structural optimizations. The elastic tensor was calculated by performing six finite distortions of the lattice and deriving the elastic constants from the strain-stress relationship [41]. Bulk

and slab calculations were performed using a 350 eV energy cut-off. The Brillouin zone was sampled with Monkhorst-Pack  $31 \times 31 \times 31$   $k$ -point meshes for bulk Al and Co,  $43 \times 43 \times 43$  and  $29 \times 29 \times 29$   $k$ -point meshes for the B2 (in the body centered cubic structure) and L1<sub>0</sub> (in the tetragonal structure) AlCo phases.

In the following all the structures are plotted using either the VESTA[42] or Rasmol[43] softwares.

### 3. Results and discussion

#### 3.1. Parameterization of the interatomic potential

The parameters ( $A, \xi, p, q$ ) for each type of bonds – Al-Al, Co-Co and Al-Co (12 parameters in total) – are mainly determined by least square mean fittings to DFT quantities like lattice parameters and cohesion or alloy formation energies. The homoatomic parameters are fitted to the cohesion energy curves of fcc Al and Co calculated with DFT as a function of the lattice parameter. For the fitting of mixed interactions, we use the formation energies of the experimentally observed ordered B2 and complex o-Al<sub>13</sub>Co<sub>4</sub> phases. With a unit cell of 102 atoms, o-Al<sub>13</sub>Co<sub>4</sub> is described by the stacking of two types of layers forming either a flat ( $F$ ) or a puckered ( $P$ ) plane as represented in Figure 1. The atoms of the cell are distributed over a sequence of four planes  $P_1F_1P_2F_2$  perpendicular to the pseudo-10-fold [100] direction.[21, 44]. Let us note that two approaches can be used to describe the o-Al<sub>13</sub>Co<sub>4</sub> crystal structure: a stacking of two types of planes, as used in this work, or of clusters. The validity of the 2D versus 3D picture has been discussed in ref. 45. According to electrical resistivity measurements, the physical properties of the compound are those of a 3D solid. Within this scheme, the stacked-layer description in terms of 2D atomic planes should be regarded as a convenient geometrical approach to describe the o-Al<sub>13</sub>Co<sub>4</sub> structure. In particular, surface science studies show that the description of o-Al<sub>13</sub>Co<sub>4</sub> as a stacking of plane is very useful to identify the surface termination [21, 44, 46]. Since this paper partly focuses on surface structures, we decided to adopt the description as a stacking of 2D planes, better adapted for our purpose.

While for pure interactions all parameters are free to vary in the fitting procedure, only  $A$  and  $\xi$  parameters are allowed to vary for the mixed inter-

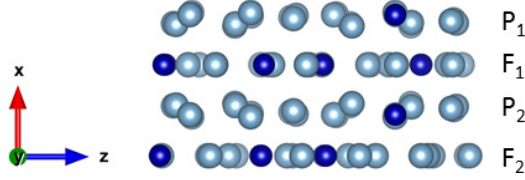


Figure 1: o- $\text{Al}_{13}\text{Co}_4$  : Bulk structure showing a periodic stacking of two types of atomic planes: flat ( $F$ ) and puckered ( $P$ ). Co and Al atoms are represented by dark and light blue balls, respectively. Four planes perpendicular to the pseudo-10-fold  $[100]$  direction ( $x$  direction) appear in a sequence  $P_1F_1P_2F_2$  (see text).

actions. In this case  $p$  and  $q$  are fixed at the arithmetic average of the values of the fcc Al and Co which may seem a rough approximation. However  $p$  and  $q$  have a physical meaning as they define the spatial range of the mixed Al-Co atomic interactions. Leaving these parameters free during the fitting procedure leads to an apparently very good fitting but at the same time to non-physical  $p$  and  $q$  values. In this sense it is more appropriate to constrain  $p$  and  $q$  parameters of the mixed interactions to intermediate values between the ones of the pure materials. This guarantees that they keep their physical meaning and that no artifact appears in the relaxed atomic structures especially at surfaces. It also insures to keep a relevant  $\frac{p}{q}$  ratio (typically  $2 < \frac{p}{q} < 5$ ) [47]. The formation energy of an  $\text{Al}_n\text{Co}_m$  alloy,  $\Delta H_f$  (eV/atom), is obtained from the total energy  $E_{\text{Al}_n\text{Co}_m}$  by using the following expression:

$$\Delta H_f = \frac{E_{\text{Al}_n\text{Co}_m} - nE_{\text{Al}}^{\text{bulk}} - mE_{\text{Co}}^{\text{bulk}}}{n + m} \quad (2)$$

where  $E_{\text{Al,Co}}^{\text{bulk}}$  is the ground state total energy per atom of Al or Co bulk material. In the SMA formulation it corresponds to the cohesive energy. The whole set of obtained parameters is given in Table 1.

$\alpha$	$\beta$	$A_{\alpha\beta}$ (eV)	$\xi_{\alpha\beta}$ (eV)	$p_{\alpha\beta}$	$q_{\alpha\beta}$
Al	Al	0.138	1.452	7.80	2.50
Co	Co	0.147	1.896	10.27	2.66
Al	Co	0.126	1.920	9.035	2.58

Table 1: SMA potential parameters for Al-Al, Co-Co and Al-Co.

Table 2 gathers the DFT and SMA calculated values of the lattice parameters and cohesive energies of the pure Al and Co materials. Some elastic constants and surface energies have been added to further check the fitted parameters. Experimental values are also given for comparison. The surface energies obtained with SMA interactions are systematically smaller than the DFT ones, which is a known effect for this type of semi-empirical potential. However the value of the difference between Al and Co surface energies is close to the DFT and experimental ones. This is essential to deal with bimetallic surfaces issues[30, 25]. The bulk modulus  $B$  and the shear moduli  $C_{44}$  and  $C'$  calculated with our model are reasonable when compared to DFT and experimental values considering the important dispersion of values found in the literature for these quantities. Most importantly all these values are found positive which is the guarantee for mechanical stability.[48]

	a (Å)	$E_{coh}$ (eV/atom)	B Mbar	$C_{44}$ Mbar	$C'$ Mbar	$E_{surf}^{(100)}$ (eV/Å <sup>2</sup> )
Al						
DFT	4.03	-3.50	0.81	0.33	0.11	0.060
SMA	4.03	-3.50	0.76	0.33	0.09	0.047
Exp.[24, 49]	4.05	-3.34	0.81	0.37	0.11	0.068
Co						
DFT	3.45	-4.97	2.60	2.07	1.11	0.150
SMA	3.45	-4.97	2.39	1.26	0.41	0.107
Exp. (fcc, thin layers)[50]	-	-	1.82	0.92	0.33	-
Exp. (hcp, bulk)[51, 49]	3.54	-4.39	1.95	0.82	-	0.157

Table 2: DFT and SMA calculated values of the lattice parameters, cohesive energies, elastic constants and surface energies of the pure materials Al and Co. The given DFT values are either the ones used in the fit lattice parameter  $a$  and cohesion energy  $E_{coh}$  or for afterwards comparison (elastic constants and surface energies). Available experimental values are also given.

Calculated equilibrium lattice parameters and formation energies for the AlCo phases used in the fit are given in Table 3 together with some experimental values.

One counterpart of the simplicity of the TB-SMA potential is the possible stabilization of ordered cubic close-packed or tetragonal phases which are

	o-Al <sub>13</sub> Co <sub>4</sub>			B2 AlCo		
	DFT	SMA	Exp. [6]	DFT	SMA	Exp. [52, 53]
$\Delta H_f$ (eV/atom)	-0.39	-0.35	-	-0.69	-0.70	-0.57
Lattice parameters (Å)	a=8.20	8.13	8.16	2.85	2.88	2.86
	b=12.40	12.35	12.34			
	c=14.42	14.44	14.45			

Table 3: Equilibrium lattice parameters and formation energies for the AlCo phases used in the fit. Available experimental values are also given.

not found in the phase diagram[54]. Here they can occur for the AlCo and Al<sub>3</sub>Co compound at or close to the composition of respectively the B2 and o-Al<sub>13</sub>Co<sub>4</sub> alloy phases. We therefore calculate the formation energies of a cubic L1<sub>2</sub> (Al<sub>3</sub>Co) and a tetragonal L1<sub>0</sub> (AlCo) ordered phases. For the L1<sub>2</sub>, very close values are obtained by DFT and with our potential, respectively -0.46 eV/atom and -0.41 eV/atom. They are both slightly lower than the energy formation of the o-Al<sub>13</sub>Co<sub>4</sub> phase which can be related to the lower Al content in Al<sub>3</sub>Co compared to o-Al<sub>13</sub>Co<sub>4</sub>. In addition o-Al<sub>13</sub>Co<sub>4</sub> is actually known to be a metastable phase at low temperature[54]. The DFT value of the formation energy obtained for the tetragonal phase L1<sub>0</sub> is -0.42 eV/atom which is, as expected, larger than the formation energy of the B2 phase. On the other hand, the tetragonal L1<sub>0</sub> is stabilized in the TB-SMA model, with a formation energy of -0.71 eV/atom, very close to the calculated formation energy for the B2 (-0.70 eV/atom). This drawback should however not alter too much the further studies on o-Al<sub>13</sub>Co<sub>4</sub>. Indeed, the important thing is the reliability of the determined potential in the concentration region of interest (here the Al-rich region).

### 3.2. Al vacancies in bulk o-Al<sub>13</sub>Co<sub>4</sub>

Following the development of the potentials for the metallic interactions, we perform a first test study of the bulk o-Al<sub>13</sub>Co<sub>4</sub> structure. From here Quenched Molecular Dynamics is used in all the simulations.

The atomic arrangements in the *F*-type and *P*-type planes, optimized by DFT and QMD, are compared in Figure 2. The characteristic patterns are almost identical in both types of atomistic simulations. After relaxation by QMD, the deviations of atomic distances in the direction perpendicular

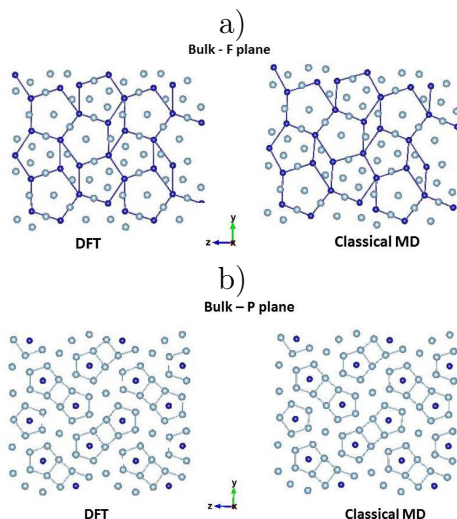


Figure 2: Results for DFT calculations (left hand side) and Classical QMD simulations (right-hand side) of bulk  $o\text{-Al}_{13}\text{Co}_4$ . a)  $F$ -type atomic plane. b)  $P$ -type atomic plane. Co and Al atoms are represented in dark and light blue, respectively, and the primary cell is repeated four times for a better visualization.

to the  $F$  and  $P$  planes show small variations of about  $\pm 0.05 \text{ \AA}$  compared to the DFT structure. The maximal fluctuations in the  $[100]$  direction for  $P$ -type planes are larger, around  $\pm 0.15 \text{ \AA}$  compared to the DFT structure but can be considered as a reasonable agreement for further use in atomistic simulations since the overall structure is well preserved. The present parameterization is therefore optimal for the bulk  $o\text{-Al}_{13}\text{Co}_4$  complex alloy despite the simplicity of the used semi-empirical potential.

As mentioned in the introduction, defects, especially Al vacancies, have a non negligible impact on the materials properties. Following the description of Mihalkovič and Widom[54], the ideal  $o\text{-Al}_{13}\text{Co}_4$  phase is a metastable structure. It becomes stable at high temperature within the introduction of a small amount of Al vacancies in the flat ( $F$ ) planes where some Co pentagons contain up to 5 Al atoms resulting in an overcrowding of Al atoms in this area. The present atomistic simulations enable a site specific analysis, in particular through local pressures. The local pressure – also named atomic stress – is given by the variation of the interaction energy  $E_{ij}$  as a function of the local deformations of the interatomic distances  $r_{ij}$ :

$$P_i = -\frac{1}{3} \sum_j \frac{dE_{ij}}{dr_{ij}} r_{ij} \quad (3)$$

Within this definition, a positive value of the local pressure corresponds to an atomic compressive stress while a negative one corresponds to an atomic tensile stress. The local pressure is calculated on each site of the system after the relaxation within the quenched MD algorithm. The stress map obtained for o-Al<sub>13</sub>Co<sub>4</sub> using a simulation crystallite containing 816 atoms is plotted in Figure 3. It clearly highlights the strongly constrained specific Al sites located only in *F*-planes (colored in red or dark orange in the right-hand side image). More precisely a stress accumulation occurs on four specific Al sites (referred as Al<sub>1</sub>-type and Al<sub>2</sub>-type) in the junction area between two contiguous Co pentagons. These sites correspond exactly to the partially occupied Al sites reported in Refs.[54, 55] pointing out precisely the area for the possible vacancy formation. Conversely, zero or negative values of the local pressure are obtained on Co sites. Since negative values correspond to a tensile stress, Co vacancy creation should not be favoured at these sites. Figure 4 shows the optimized structures obtained after relaxation by quenched MD for a structure obtained after removing one Al<sub>1</sub>-type (left image) or one Al<sub>2</sub>-type (right image) atom at the most stressed sites in an *F*-plane. Such removal allows the system to actually release a large amount of its stress since the local pressures strongly decrease around the place where the vacancy was created. At first sight, removing one Al<sub>2</sub>-type atom seems to be slightly more favorable since the local pressures tend towards zero within a larger area.

The vacancy energetics can be also examined per site in the whole bulk compound. The vacancy energy formation is calculated within the equation:

$$E_{for}^{vac} = E_{N-1} + E_{Al}^{Al_{13}Co_4} - E_N \quad (4)$$

where  $E_{N-1}$  is the total energy of the crystallite with one vacancy and  $E_N$  the total energy of the ideal bulk with N atoms.  $E_{Al}^{Al_{13}Co_4}$  is the accessible site energy (or cohesive energy) of the corresponding removed atom initially in the bulk o-Al<sub>13</sub>Co<sub>4</sub> compound. The vacancy formation energies calculated for all the Al atomic sites of the compound are gathered in the graph of Figure 5. The results are consistent with the preferential vacancy formation in the

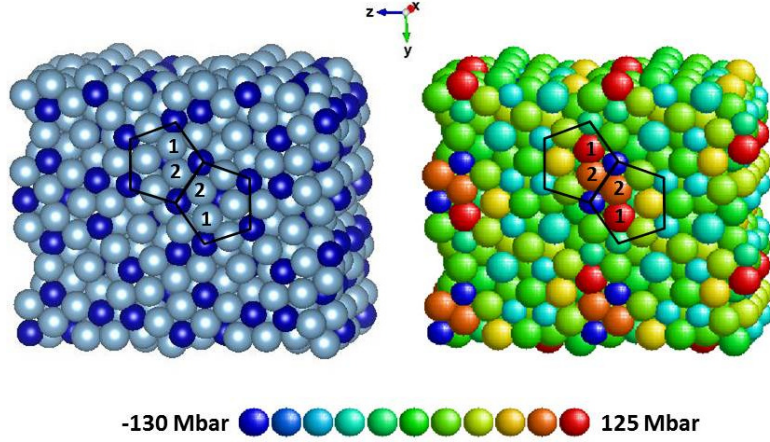


Figure 3: Left image : bulk atomic structure of  $o\text{-Al}_{13}\text{Co}_4$  (crystallite of 816 atoms) obtained after relaxation at 0 K by QMD. The front plane is of  $F$ -type. Dark blue and light blue balls correspond respectively to Co and Al atoms. Right image : Atomic stress on each site of the same structure. The bottom picture illustrates the used color code in the right hand side atomic structure, going from the maximal value of pressure (red) to the minimal one (blue). In both crystallites the two black pentagons connect five Co atoms, while sharing two Co atoms by one of their edges. The most compressed Al atoms are referred as (1) and (2).

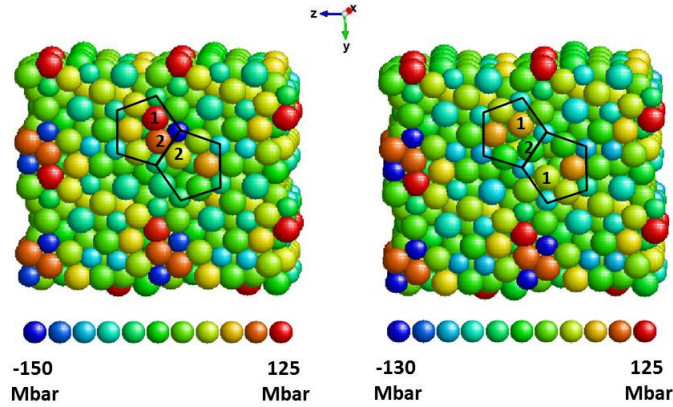


Figure 4: Optimized bulk atomic structures of  $o\text{-Al}_{13}\text{Co}_4$  (crystallite of 815 atoms) obtained by QMD after removing one  $\text{Al}_1$ -type atom from the ideal structure (left image) or one  $\text{Al}_2$ -type atom (right image). Large and small balls correspond to Al and Co atoms respectively. The bottom pictures illustrate the used color code in the atomic structures, going from the maximal value of pressure (red) to the minimal one (blue).

most compressed regions. First the vacancy formation is favored in  $F$  planes. Then the lower energy (+0.29 eV/atom) is obtained when one  $\text{Al}_2$ -type atom is removed. A higher, although rather close, energy (+0.36 eV/atom) is obtained when removing one  $\text{Al}_1$ -type atom. This is in agreement with the optimal stress release obtained when an  $\text{Al}_2$ -type atom is removed compared to  $\text{Al}_1$  (see Figure 4).

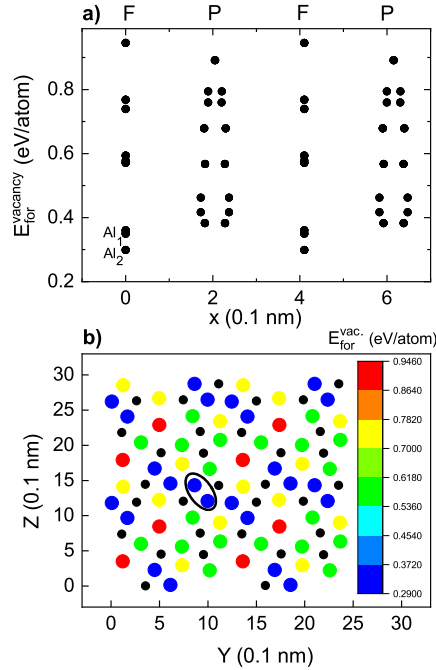


Figure 5: Al vacancy formation energies per site in bulk  $\text{o-Al}_{13}\text{Co}_4$ . a) Representation along the direction perpendicular to the alternating  $F$ - and  $P$ - planes. b) Mapping of the Al vacancy formation energies in one  $F$ -plane. The scale on the right hand side of the graph illustrates the used color code, going from the smallest values of energies (blue) to the largest ones (red). The black ellipse contains two circles corresponding to  $\text{Al}_2$ -type sites. The positions of Co atoms have been marked by small black circles for a better visualization of the structure.

This case study shows that the mapping of the local pressure provides a good guide for locating precisely the areas where vacancies could be formed. It is worth noticing that both sterical and electronic structure effects are at play in the vacancy formation and the stabilization of the resulting  $\text{o-Al}_{13}\text{Co}_4$  compound[54]. Although electronic effects could hardly be taken

into account within our atomistic approach, we show here the importance of stress relaxation in the vacancy formation.

### 3.3. *o*-Al<sub>13</sub>Co<sub>4</sub>(100) surface

After showing the reliability of the TB-SMA model for point defects, we move to the case of extended defects illustrated here by the investigation of the pseudo-10-fold surface of *o*-Al<sub>13</sub>Co<sub>4</sub>(100). According to previous experimental studies, the surface termination is found to derive from the *P*-type planes only, which present a higher atomic density and a higher concentration of Al than the flat planes[21, 44]. The corresponding surface termination has a unit cell defined as follows: it contains four Co atoms per surface unit cell (model  $S_1$  in Figure 6), two of them are located above the mean position of the puckered layer, while the other two are located below. Following previous works[21] we consider several variations of the *P*-termination model (considering only  $P_2$  from the two equivalent  $P_1$  and  $P_2$  planes). The main structures are represented in Figures 6 and 7 where the upper images are the structures optimized by DFT and the lower ones are the structures relaxed by QMD. More precisely, Figure 6 shows the four models of the complete (or almost complete) *P*-termination model, including four Co atoms ( $S_1$ ), only the two protruding Co atoms ( $S_2$ ), only the two Co atoms located slightly below the mean position of the termination plane ( $S_3$ ), and no Co atoms ( $S_4$ ). Figure 7 shows four other possible models based on an incomplete *P*-termination model in which only one set of bipentagons is present, leading to much less dense surfaces. These models are named:  $S_5$  with bipentagons containing the top Co atoms,  $S_{5-2Co}$  with the same bipentagons and two missing top Co atoms,  $S_6$  with bipentagons containing the bottom Co atoms and  $S_{6-2Co}$  with the same bipentagons and two missing Co atoms.

The relative surface energies  $\gamma_{surf} - \gamma_{surf}^{S_1}$  are also evaluated, from the total energies obtained within the QMD simulations. They are represented in Figure 8 as a function of the chemical potential variation  $\mu_{Al} - \mu_{Al}^{bulk}$ . In this representation the relevant values of the relative surface energies are obtained within the range of chemical potential respecting the condition:  $\frac{\Delta H_f}{13} \leq \mu_{Al} - \mu_{Al}^{bulk} \leq 0$ . It is worth noticing that we use here the same formulation of the relative surface energies and the same representation as in Ref. 21. This facilitates the comparison with the previous literature.

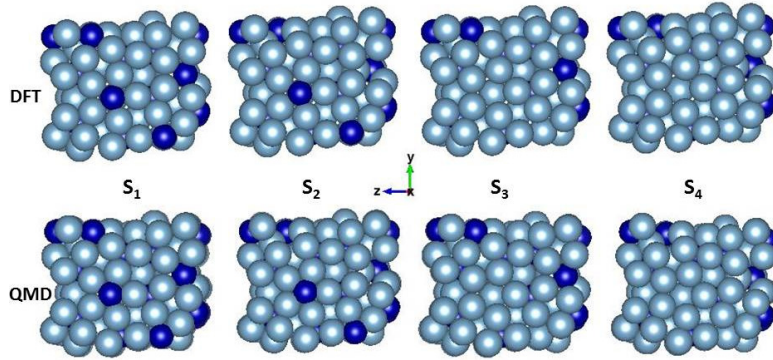


Figure 6: Model structures of  $P_2$ -termination (almost complete). The models numbered from 1 to 4 are the denser ones for this surface. Dark blue and light blue balls correspond respectively to Co and Al atoms. The upper images correspond to the structures optimized with DFT and the lower ones to the same structures further relaxed by classical QMD.

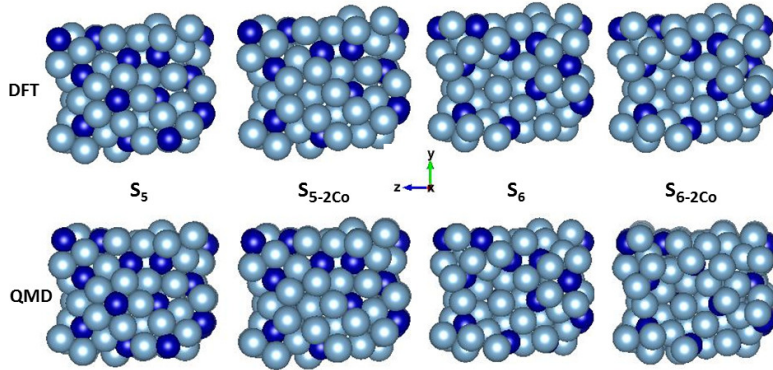


Figure 7: Incomplete surface terminations for the  $P_2$  layer. Dark blue and light blue balls correspond to Co and Al atoms respectively. The upper images correspond to the structures optimized by DFT and the lower ones to the same structures further relaxed by classical QMD.

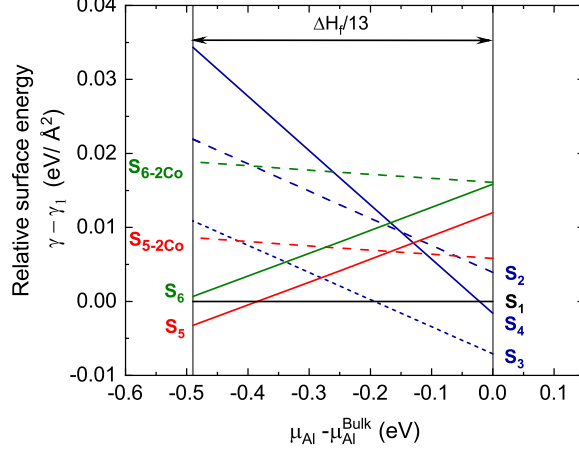


Figure 8: Relative surface energy *vs* the chemical potential  $\mu_{Al} - \mu_{Al}^{bulk}$  for the different models of Figures 6 and 7.

Generally the QMD results are rather consistent with DFT and experimental observations. At first sight, the most stable models are  $S_3$ ,  $S_1$  and  $S_5$ ,  $S_4$  being between  $S_1$  and  $S_3$  in terms of relative surface energies and only on a very small range of chemical potentials. In general the relative stability to  $S_1$  strongly depends on the chemical potential. The  $S_3$  model is found to be the most stable within a large domain of chemical potentials on the right hand side of the diagram ( $\mu_{Al} - \mu_{Al}^{bulk} > -0.2$  eV) *i.e* in the region where the chemical potential of Al in  $\alpha\text{-Al}_{13}\text{Co}_4$  is close to the one of Al in fcc Al. This model which corresponds to a dense *P*-type termination where the two protruding Co atoms have been removed, is also the one experimentally observed under ultra-high vacuum conditions by surface science studies [21, 22]. Within the QMD simulations, the two remaining bottom Co atoms tend to sink into the surface in agreement with a previous study[44]. Both effects, vacancy of Co protruding atoms and sinking of remaining Co surface atoms, can be related to the much higher energy of pure Co close-packed surfaces compared to Al ones. In DFT calculations, the  $S_4$  model, with all Co atoms removed, is found to compete with  $S_3$ [21]. In our case the relative energy of  $S_4$  remains above the one of  $S_3$  probably because the denser situation (preserving the cohesion with less broken bonds) is finally favored. Then the system can lower its energy by a sinking of Co bottom atoms deeper

inside the surface layer. In this series of dense surfaces, the surface energies of  $S_2$  and  $S_3$  as a function of the Al chemical potential present similar slopes because the surface composition is similar in both models. On the contrary to  $S_3$ , the  $S_2$  structure takes positive relative surface energy values in the whole range of considered chemical potentials which can be related to the presence of protruding Co atoms in this model. In summary, at least within our model, there is a competition at surfaces between preserving the cohesion by minimizing the number of broken bonds and avoiding the presence of Co atoms at the surface. On the left hand side of the diagram, the relative surface energy of the  $S_5$  model, belonging to the family of the so-called cluster preserving (or Henley clusters) models [22], has apparently the same trends as in DFT calculations but it is found to be the most stable on a smaller range of chemical potential ( $\frac{\Delta H_f}{13} \leq \mu_{Al} - \mu_{Al}^{bulk} \leq -0.4$  eV). It is however very satisfying that the relaxed configuration by classical QMD well preserves the initial pattern. The other less dense structures  $S_{5-2Co}$  and  $S_6$  are also well preserved after QMD simulations. Lateral displacements of Al atoms from their initial positions are however visible in the relaxed  $S_{6-2Co}$  structure. They are driven by the tendency of Al atoms to cover underlying Co atoms. Within the classical QMD relaxation based on our TB-SMA potential, these displacements are favored by the fact that Al atoms are much less bonded in these less dense surface structures. The same behavior is not observed for the  $S_{5-2Co}$  where top Co atoms are removed while bottom Co are removed from  $S_6$  to obtain  $S_{6-2Co}$  leading to a destabilization of the structure as seen also from the surface energy diagram.  $S_{5-2Co}$  and  $S_6$  model structures, although preserved in the simulations, have however positive relative surface energies on the whole range of considered chemical potentials. Finally, in this series the cluster preserving model with Co atoms at their top is therefore the most stable in agreement with Ref. 22.

#### 4. Conclusion

We have parameterized an N-body potential based on the tight-binding second moment approximation to describe atomic interactions in o-Al<sub>13</sub>Co<sub>4</sub>. This potential has been implemented in classical quenched molecular dynamics simulations for structural studies of the realistic complex compound in the presence of defects, either point (vacancies) or extended (surfaces). Considering the inherent qualitative nature of such studies compared to DFT, most of the physics of the complex o-Al<sub>13</sub>Co<sub>4</sub> compound was well captured. The

TB-SMA model was shown to be reliable in the bulk by preserving the cluster structure of the  $\text{o-Al}_{13}\text{Co}_4$  complex alloy phase. Then, the importance of stress relaxation in vacancy formation was highlighted through the mappings of local pressures and the calculation of vacancy formation energies. The two types of most compressed Al sites in the bulk flat planes correspond exactly to the sites for which the vacancy formation energies are the lowest. Thanks to the N-body character of the potential, the investigation of surfaces could be tackled which was not done before in atomistic studies of this complex phase. The calculation of the relative surface energies gives the same trends as DFT calculations. The analysis of the relaxed tested configurations emphasizes the competition between preserving the cohesion by minimizing the number of broken bonds and avoiding the presence of Co atoms at the surface. Important perspectives can then be envisaged using a complex  $\text{o-Al}_{13}\text{Co}_4$  substrate, in particular large scale simulations of inaccessible phenomena until now, such as growth, wetting or large scale self-assembling. Apart from the surfaces, extended defects include also metadislocations which are associated with separate phason defects. The latter escort the movement of the metadislocations through the material. The development of TB-SMA potentials, able to correctly describe point and plane defects, may help the investigation of extended metadislocations. Indeed, atomic models for metadislocation glide motion, are based on atomic diffusion, as demonstrated by ref. 56. In addition, the development of the efficient TB-SMA potential may be further used to understand the interaction between metadislocations and vacancies, which likely plays an important role in the transformation from an orthorhombic to a monoclinic phase.

### **Data Availability**

The raw and processed data required to reproduce these findings are available from the authors upon request.

### **Acknowledgements**

This work was funded by the French National Research Agency (ANR) through the Programme d'Investissement d'Avenir under contract ANR-11-LABX-0058 NIE within the Investissement d'Avenir program ANR-10-IDEX-

0002-02. It is also supported by the European Integrated Center for the Development of New Metallic Alloys and Compounds. Some of us acknowledge financial support through the COMETE project (COncEption in silico de Matériaux pour l'Environnement et l'Énergie) co-funded by the European Union under the program FEDER-FSE Lorraine et Massif des Vosges 2014-2020. High Performance Computing resources were provided by GENCI under the allocation 99642, as well as the EXPLOR center hosted by the Université de Lorraine (allocation2017M4XXX0108).

## References

- [1] J. Dolinšek, M. Komelj, P. Jeglič, S. Vrtnik, D. Stanić, P. Popčević, J. Ivkov, A. Smontara, Z. Jagličič, P. Gille, Y. Grin, Anisotropic magnetic and transport properties of orthorhombic  $\text{Al}_{13}\text{Co}_4$ , *Phys. Rev. B* 79 (2009) 184201.
- [2] M. Armbrüster, K. Kovnir, M. Friedrich, D. Teschner, G. Wowsnick, M. Hahne, P. Gille, L. Szentmiklosi, M. Feuerbacher, M. Heggen, F. Girgsdies, D. Rosenthal, R. Schlögl, Y. Grin,  $\text{Al}_{13}\text{Fe}_4$  as a Low-Cost Alternative for Palladium in Heterogeneous Hydrogenation, *Nat. Mater.* 11 (2012) 690–693.
- [3] L. Piccolo, C. Chatelier, M.-C. de Weerd, F. Morfin, J. Ledieu, V. Fournée, P. Gille, E. Gaudry, Catalytic Properties of  $\text{Al}_{13}\text{TM}_4$  Complex Intermetallics: Influence of the Transition Metal and the Surface Orientation on Butadiene Hydrogenation, *Sci. Tech. Adv. Mater.* 20 (2019) 557–567.
- [4] K. Anand, V. Fournée, G. Prévôt, J. Ledieu, E. Gaudry, Non-Wetting Behavior of Al-Co Quasicrystalline Approximants Owing to their Unique Electronic Structures, *ACS Appl. Mater. Interfaces* 12 (2020) 15793–15801.
- [5] P.-F. Lory, V. M. Giordano, P. Gille, H. Euchner, M. Mihalkovič, E. Pellegrini, M. Gonzalez, L.-P. Regnault, P. Bastie, H. Schober, S. Pailhes, M. R. Johnson, Y. Grin, M. de Boissieu, Impact of Structural Complexity and Disorder on Lattice Dynamics and Thermal Conductivity in the o- $\text{Al}_{13}\text{Co}_4$  phase, *Phys. Rev. B* 102 (2020) 024303.

- [6] J. Grin, U. Burkhardt, M. Ellner, K. Peters, Crystal Structure of Orthorhombic  $\text{Co}_4\text{Al}_{13}$ , *J. Alloys Comp.* 206 (1994) 243–247.
- [7] X. L. Ma, K. H. Kuo, Decagonal quasicrystal and related crystalline phases in slowly solidified Al-Co alloys, *Metallurgical Transactions A* 23 (1992) 1121–1128.
- [8] J. M. Dubois, Properties and Applications of Quasicrystals and Complex Metallic Alloys, *Chem. Soc. Rev.* 41 (2012) 6760–6777.
- [9] P. Simon, I. Zelenina, R. Ramlau, W. Carrillo-Cabrera, U. Burkhardt, H. Borrmann, R. Cardoso-Gil, M. Feuerbacher, P. Gille, Y. Grin, Structural Complexity of the Intermetallic Compound  $\text{o-Al}_{13}\text{Co}_4$ , *J. Alloys Comp.* 820 (2020) 153363.
- [10] M. Widom, J. A. Moriarty, First-Principles Interatomic Potentials for Transition-Metal Aluminides. II. Application to Al-Co and Al-Ni Phase Diagrams, *Phys. Rev. B* 58 (1998) 8967–8979.
- [11] M. Widom, I. Al-Lehyani, J. A. Moriarty, First-principles Interatomic Potentials for Transition-Metal Aluminides. III. Extension to Ternary Phase Diagrams, *Phys. Rev. B* 62 (2000) 3648.
- [12] J.-B. S. M. Mihalkovič, H. Elhor, Low-energy Phonon Excitations in the Decagonal Quasicrystal  $\text{Al}_{70}\text{Co}_{15}\text{Ni}_{15}$  and in crystalline  $\text{Al}_{13}\text{Co}_4$  phases, *Mater. Sci. Eng., A* 294-296 (2000) 654–657.
- [13] M. Mihalkovič, C. L. Henley, Empirical Oscillating Potentials for Alloys from ab initio Fits and the Prediction of Quasicrystal-related Structures in the Al-Cu-Sc System, *Phys. Rev. B* 85 (2012) 092102.
- [14] C. Chatelier, Y. Garreau, L. Piccolo, A. Vlad, A. Resta, J. Ledieu, V. Fournée, M.-C. de Weerd, F.-E. Picca, M. de Boissieu, R. Felici, A. Coati, E. Gaudry, From the Surface Structure to Catalytic Properties of  $\text{Al}_5\text{Co}_2(2-10)$ : A Study Combining Experimental and Theoretical Approaches, *J. Phys. Chem. C* 124 (2020) 4552–4562.
- [15] P. Šulhříek, M. Drienovský, I. Černíčková, L. L. Ďuriška, R. Skaudžius, Z. Gerhátová, M. Palcut, Oxidation of Al-Co Alloys at High Temperatures, *Materials* 13 (2020) 3152.

- [16] R. Phillips, J. Zou, A. E. Carlsson, M. Widom, Electronic-Structure-Based Pair Potentials for Aluminum-Rich Cobalt Compounds, *Phys. Rev. B* 49 (1994) 9322.
- [17] W.-P. Dong, H.-K. Kim, W.-S. Ko, B.-M. Lee, B.-J. Lee, Atomistic Modeling of Pure Co and Co-Al System, *Calphad* 38 (2012) 7–16.
- [18] G. Purja-Pun, V. Yamakov, Y. Mishin, Interatomic Potential for the Ternary Ni-Al-Co System and Application to Atomistic Modeling of the B2-L10 Martensitic Transformation, *Modelling Simul. Mater. Sci. Eng.* 23 (2015) 065006.
- [19] C. Vailhé, D. Farkas, Shear Faults and Dislocation Core Structures in B2 CoAl, *Journal of Materials Research* 12 (1997) 2559–2570.
- [20] S. Alarcón Villaseca, J. Ledieu, L. N. Serkovic Loli, M. C. de Weerd, P. Gille, V. Fournée, J. M. Dubois, E. Gaudry, Structural Investigation of the (001) Surface of the Al<sub>9</sub>Co<sub>2</sub> Complex Metallic Alloy, *J. Phys. Chem. C* 115 (2011) 14922–14932.
- [21] H. Shin, K. Pussi, E. Gaudry, J. Ledieu, V. Fournée, S. A. Villaseca, J. Dubois, Y. Grin, P. Gille, W. Moritz, Structure of the Orthorhombic Al<sub>13</sub>Co<sub>4</sub> ( 100 ) Surface Using LEED , STM and ab initio Studies, *Phys. Rev. B* 84 (2011) 085411.
- [22] P. Scheid, C. Chatelier, J. Ledieu, V. Fournée, E. Gaudry, Bonding Network and Stability of Clusters : the Case Study of Al<sub>13</sub>TM<sub>4</sub> Pseudo-Tenfold Surfaces, *Acta Cryst. A* 75 (2019) 314–324.
- [23] V. Rosato, M. Guillopé, B. Legrand, Thermodynamical and Structural Properties of F.C.C. Transition Metals Using a Simple Tight-Binding Model, *Phil. Mag. A* 59 (1989) 321–336.
- [24] F. Cleri, V. Rosato, Tight-Binding Potentials for Transition Metals and Alloys, *Phys. Rev. B* 48 (1993) 22–33.
- [25] C. Goyhenex, Revised Tight-Binding Second Moment Potential for Transition Metal Surfaces, *Surf. Sci.* 3-4 (2012) 325–328.
- [26] N. I. Papanicolaou, G. C. Kallinteris, G. A. Evangelakis, Second-Moment Interatomic Potential for Aluminum Derived from Total-Energy

- Calculations and Molecular Dynamics Application, *Comput. Mater. Sci.* 17 (2000) 224–229.
- [27] N. I. Papanicolaou, H. Chamati, G. A. Evangelakis, Second-Moment Interatomic Potential for Al, Ni and Ni – Al alloys, and Molecular Dynamics Application, *Comput. Mater. Sci.* 27 (2003) 191–198.
- [28] S. H. Yang, M. J. Mehl, D. Papaconstantopoulos, Application of a Tight-Binding Total-Energy Method for Al, Ga, and In, *Phys. Rev. B* 57 (4) (1998) R2013–R2016.
- [29] B. Legrand, M. Guillopé, J. S. Luo, Multilayer Relaxation and Reconstruction in BCC and FCC Transition and Noble Metals, *Vacuum* 41 (6) (1990) 311–314.
- [30] C. Goyhenex, H. Bulou, J.-P. Deville, G. Tréglia, Pt/Co(0001) Superstructures in the Submonolayer Range: A Tight-Binding Quenched-Molecular-Dynamics Study, *Phys. Rev. B* 60 (4) (1999) 2781–2788.
- [31] H. Bulou, C. Goyhenex, Surface Mismatch and Stress Relief Mechanisms at Metallic Surfaces, *Appl. Surf. Sci.* 188 (2002) 163–169.
- [32] I. Chado, C. Goyhenex, H. Bulou, J. Bucher, Evolution of the Morphology of Small Co Clusters Grown on Au(1 1 1), *Appl. Surf. Sci.* 226 (2004) 178–184.
- [33] G. Kresse, J. Hafner, Ab Initio Molecular Dynamics for Liquid Metals, *Phys. Rev. B* 47 (1993) 558–561.
- [34] G. Kresse, J. Hafner, Ab Initio Molecular-Dynamics Simulation of the Liquid-Metal-Amorphous-Semiconductor Transition in Germanium, *Phys. Rev. B* 49 (1994) 14251–14269.
- [35] G. Kresse, J. Furthmüller, Efficient Iterative Schemes for Ab Initio Total-Energy Calculations Using A Plane-Wave Basis Set, *Phys. Rev. B* 54 (1996) 11169 – 11186.
- [36] G. Kresse, J. Furthmüller, Efficiency of Ab-Initio Total Energy Calculations For Metals and Semiconductors Using a Plane Wave Basis Set, *Comput. Mater. Sci.* 6 (1996) 15–50.

- [37] P. E. Blochl, Projector Augmented-Wave Method, *Phys. Rev. B* 50 (1994) 17953–17979.
- [38] G. Kresse, D. Joubert, From Ultrasoft Pseudopotentials To the Projector Augmented-Wave Method, *Phys. Rev. B* 59 (1999) 1758–1775.
- [39] J. P. Perdew, K. Burke, M. Ernzerhof, Generalized Gradient Approximation Made Simple, *Phys. Rev. Lett.* 77 (1996) 3865.
- [40] J. P. Perdew, K. Burke, M. Ernzerhof, Erratum: Generalized gradient approximation made simple, *Phys. Rev. Lett.* 78 (1997) 1396.
- [41] Y. L. Page, P. Saxe, Symmetry-General Least-Squares Extraction of Elastic Data for Strained Materials from ab initio Calculations of Stress, *Phys. Rev. B* 65 (2002) 104104.
- [42] K. Momma, F. Izumi, VESTA 3 for Three-Dimensional Visualization of Crystal, Volumetric and Morphology Data, *J. Appl. Crystallogr.* 44 (2011) 1272–1276.
- [43] R. Sayle, E. J. Milner-White, RasMol: Biomolecular graphics for all, *Trends in Biochemical Sciences (TIBS)* 20 (1995) 374.
- [44] E. Gaudry, C. Chatelier, G. Mcguirk, L. S. Loli, M.-c. D. Weerd, J. Ledieu, V. Fournée, R. Felici, J. Drnec, G. Beutier, M. de Boissieu, Structure of the  $\text{Al}_{13}\text{Co}_4$  (100) Surface : Combination of Surface X-Ray Diffraction and ab initio Calculations, *Phys. Rev. B* 94 (2016) 165406.
- [45] J. Dolinšek, A. Smontara, Decagonal Quasicrystals and Approximants: Two-Dimensional or Three-Dimensional Solids?, *Isr. J. Chem.* 51 (2011) 1246–1256.
- [46] V. Fournée, E. Gaudry, M.-C. de Weerd, R. D. Diehl, J. Ledieu, The (100) surface of the  $\text{Al}_{13}\text{Co}_4$  quasicrystalline approximant, *MRS Proceedings* 1517 (2013) mrsf12–1517–kk02–07.
- [47] F. Ducastelle, Modules Élastiques des Métaux de Transition, *J. Phys.* 31 (1970) 1055–1062.
- [48] M. Born, K. Huang, *Dynamical Theory of Crystal Lattices*, Oxford University Press, 1954.

- [49] W. R. Tyson, W. A. Miller, Surface Free Energies of Solid Metals, *Surf. Sci.* 62 (1977) 267–276.
- [50] J. Gump, X. Hua, M. C. M, R. Sooryakumarb, M. A. Tomaz, G. R. Harp, Elastic Constants of Face-Centered-Cubic Cobalt, *J. Appl. Phys.* 86 (1999) 6005–6009.
- [51] G. Simmons, H. Wang, Single Crystal Elastic Constants and Calculated Aggregate Properties: a Handbook, MIT Press, 1971.
- [52] W. F. Gale, T. C. Totemeir, *Smithells Metals Reference Book*, 8th ed, Amsterdam: Elsevier, 2004.
- [53] R. Hultgren, R. L. Orr, P. D. Anderson, K. K. Kelley, *Selected Values of the Thermodynamic Properties of Metals and Alloy*, New York: Wiley, 1963.
- [54] M. Mihalkovič, M. Widom, First-Principles Calculations of Cohesive Energies in the Al-Co Binary Alloy System, *Phys. Rev. B* 75 (2007) 014207.
- [55] P. Lory, V. M. Giordano, P. Gille, H. Euchner, M. Mihalkovič, E. Pellegrini, M. Gonzalez, L. Regnault, Impact of Structural Complexity and Disorder on Lattice Dynamics and Thermal Conductivity in the  $\alpha$ -Al<sub>13</sub>Co<sub>4</sub> phase, *Phys. Rev. B* 102 (2020) 024303.
- [56] M. Heggen, M. Feuerbach, Core Structure and Motion of Metadislocations in the Orthorhombic Structurally Complex Alloy Al<sub>13</sub>Co<sub>4</sub>, *Mater. Res. Lett.* 2:3 (2014) 146–151.